Nonlinear Dynamics and Systems Theory, **21** (5) (2021) 471–480

Dynamics of Nonlinearly Damped Duffing-Van Der Pol Oscillator Driven by Frequency Modulated Signal

B. Bhuvaneshwari [1], S. Valli Priyatharsini [1], V. Chinnathambi [1,*] and S. Rajasekar [2]

[1] *Department of Physics, Sadakathullah Appa College, Tirunelveli 627 011, Tamil Nadu, India.*
[2] *School of Physics, Bharathidasan University, Tiruchirapalli 620 024, Tamilnadu, India.*

Received: July 13, 2019; Revised: September 10, 2021

Abstract: The dynamics of a nonlinearly damped Duffing-Van der Pol (DVP) oscillator driven by a frequency modulated (FM) signal is numerically investigated as a function of the amplitude (g) and frequency (Ω) of the high-frequency signal and damping exponent (P). FM signals are basically classified into two types, namely, Narrow-Band FM (NBFM) and Wide-Band FM (WBFM). We considered both signals to study the dynamics of the system. As the amplitude g and frequency Ω of the high-frequency signal are varied, with other parameters at a constant value, a variety of features such as different routes to chaos, periodic windows, period-doubling and reverse period-doubling bifurcations, periodic bubbles, hysteresis and vibrational resonance are found to occur due to the signals. Our results show many striking departures from the behaviour of a linearly damped system with the FM signal. A bifurcation diagram, phase portrait, Poincaré map, resonance plot are also plotted to show the manifestation of periodic and chaotic orbits and resonance phenomenon.

Keywords: *DVP oscillator; nonlinear damping; FM signal; hysteresis; chaos; vibrational resonance.*

Mathematics Subject Classification (2010): 34C55, 34C25, 37D45, 37G35, 70K30.

* Corresponding author: mailto:veerchinnathambi@gmail.com

1 Introduction

There have been enormous contributions to the study of the dynamical behaviours in linearly damped and driven dynamical systems, including various routes to chaos, crises and resonance phenomenon [1–4]. However, there is a need for research on various dynamical behaviours in nonlinearly damped driven dynamical systems. Exploring the features of various dynamics in systems with different types of setup of the external force is of great importance. Recently, Cheib et al. [5] studied the dynamics of a two-degree-of-freedom nonlinear mechanical system under the action of harmonic excitation. Khachnaoni [6] investigated the existence of homoclinic orbits for damped vibration system with small forcing terms and Kyziol and Okninski [7] found the periodic steady-state solutions of the periodically driven Duffing-Van der Pol oscillator using the Krylov-Bogoliubov-Mitropolsky approach. It is of considerable interest to study the system under the influence of FM signal. The study of such signal will be helpful in creating and controlling nonlinear dynamical behaviours [8–10]. The nonlinear damping term is taken to be proportional to the power of the velocity in the form $\gamma\dot{x} \mid \dot{x} \mid^{P-1}$. A similar nonlinear damping term was used previously by researchers [3, 11–13].

The FM signal is basically classified into two types, namely, Narrow Band FM (NBFM) and Wide Band FM (WBFM) or Broad band FM. An NBFM signal is the FM signal with a smaller bandwidth. The modulation index (M_f) of the NBFM signal is small as compared to one radian. Hence the spectrum of the NBFM signal consists of the carrier and upper and lower side-bands. The NBFM signal can be expressed mathematically as

$$S_1(t) = f(\cos\omega t - g\sin\Omega t\sin\omega t),\ \Omega >> \omega, \tag{1a}$$

where the amplitude f of the low-frequency (ω) periodic signal is modulated by the high-frequency (Ω) periodic signal with amplitude g. With the use of the formula $\sin\Omega t\sin\omega t = \frac{1}{2}[\cos(\Omega-\omega) - \cos(\Omega+\omega)]$, it takes the form

$$S_1(t) = f\cos\omega t + \frac{fg}{2}\left[\cos(\Omega+\omega)t - \cos(\Omega-\omega)t\right],\ \Omega >> \omega. \tag{1b}$$

When $\Omega >> \omega$, the frequency modulated signal can also be treated as consisting of a low-frequency signal $f\cos\omega t$ and two high-frequency signals with frequencies $(\Omega+\omega)$ and $(\Omega-\omega)$. This signal is used in FM mobile communications such as police wireless, ambulances, taxicabs, etc. For large value of the modulation index, the FM signal ideally contains the carrier and an infinite number of side bands located symmetrically around the carrier. Such an FM signal has infinite bandwidths and is called the Wide Band FM (WBFM) signal. The modulation index of the WBFM is higher than 1. This signal is used in the entertainment broadcasting applications such as FM radio, TV etc. The expression for the WBFM signal is complex since it is sine of sine function. The only way to solve this equation is by using the Bessels function. The mathematical expression for the WBFM signal is

$$S_2(t) = f\sin(\omega t + g\sin\Omega t),\ \Omega >> \omega. \tag{2}$$

The equation of motion of a nonlinearly damped DVP oscillator with the NBFM signal is given by

$$\ddot{x} + \gamma\dot{x}(1-x^2) \mid \dot{x} \mid^{P-1} -\alpha^2 x + \beta x^3 = S_1(t) \tag{3}$$

and with the WBFM signal is given by

$$\ddot{x} + \gamma\dot{x}(1 - x^2) \mid \dot{x} \mid^{P-1} -\alpha^2 x + \beta x^3 = S_2(t), \tag{4}$$

where α is the natural frequency, β is the constant parameter which plays the role of a nonlinear parameter, $\gamma > 0$ is the damping parameter of the system, P is the damping exponent, $S_1(t)$ and $S_2(t)$ are the NBFM and WBFM signals. Recently, many researchers used these signals to analyze the dynamical behaviours of various dynamical systems [8–10]. In the present study, we wish to numerically analyze the dynamical behaviours in a nonlinearly damped DVP oscillator driven by the NBFM and WBFM signals.

The paper is structured as follows. Section 2 gives the dynamical behaviours of a nonlinearly damped DVP oscillator subjected to the NBFM signal. We show the occurrence of various dynamical behaviours such as bifurcations and chaos, hysteresis and vibrational resonance phenomena due to the presence of the NBFM signal. We take up the system with the WBFM signal in Section 3. Finally, the conclusion of the research work is given in Section 4.

2 Dynamical Behaviours of the System with NBFM Signal

2.1 Bifurcations and chaos

The aim of this section is to seek numerically the dynamical behaviours of the system (Eq.(3)) when the control parameter g evolves for different values of the damping exponent P. When the control parameter g is varied and a bifurcation takes place, a qualitative change of the system happens.

Eq.(3) and Eq.(4) are solved by the fourth-order Runge-Kutta method with the time step size $\Delta t = (2\pi/\omega)/1000$. The initial conditions in the numerical calculations are fixed at $x(0) = 0.1$ and $\dot{x}(0) = 0.0$. Numerical solutions corresponding to first 500 drive cycles are left as transient. We analysed the behaviour of the systems (Eq.(3) and Eq.(4)) by varying the amplitude g of the signals with the fixed values of f, ω and Ω. The numerical results are demonstrated through the bifurcation diagram, phase portrait, Poincaré map and response amplitude. For our numerical computation, we fix the parameters at α=1.0, β=5.0, γ=0.4, ω=0.1,Ω=5.0, P=1.0,1.5 and 2.0 and the signal amplitudes f and g are varied from small values. From our numerical analysis, we find the following.

First, we show the effect of the control parameter g with the fixed value of f=0.2 and P=1.0,1.5 and 2.0. Fig.1 shows the bifurcation diagram of the system (Eq.(3)) with f=0.2 and P=1.0,1.5 and 2.0. In Fig.1(a), for P=1.0 no chaotic behaviour is observed. But for P=1.5 and 2.0 various dynamical behaviours such as a period-doubling bifurcation leading to chaotic behaviour, periodic windows and a reverse period-doubling bifurcation occur, which is clearly evident in Fig.1(b) and Fig.1(c). Magnification of a part of the bifurcation diagram of Fig.1(c) is shown in Fig.1(d). Fig.1(d) shows the bifurcation diagram where f is set to 0.2 and P=2.0, while g is varied. For small values of g the coexistence of two limit cycle orbits occurs. As the parameter g is increased, both the orbits exhibit a transcritical bifurcation and a cascade of period-doubling bifurcation leading to chaotic motion. A transcritical bifurcation occurs at g=2.3174. The period-1,2,4,8 and 16 orbits are found in the intervals (0-2.4055), (2.4055-2.4481), (2.4481-2.4588), (2.4588-2.4603) and (2.4603-2.4626), respectively. The onset of chaos is found at f=2.4632. An example of the chaotic orbit at $g = 2.95$ and the corresponding Poincaré map are shown

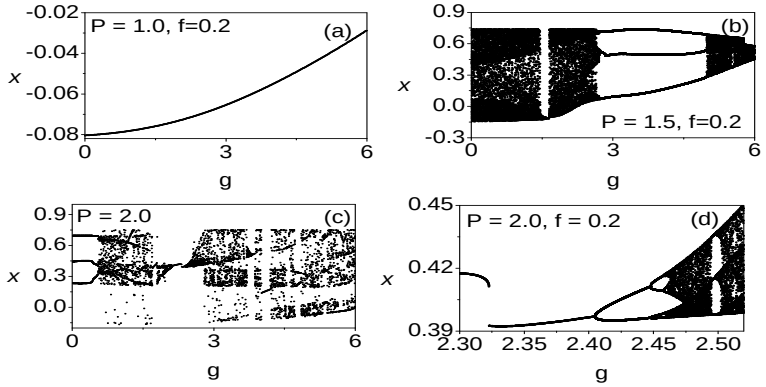

Figure 1: (a-c) Bifurcation diagrams for few values of P with $f = 0.2$. (d) Magnification of a part of the bifurcation diagram of Fig.1(c). The other parameter values are $\alpha = 1.0,\ \beta = 5.0,\ \gamma = 0.4,\ \Omega = 5.0$ and $\omega = 0.1$.

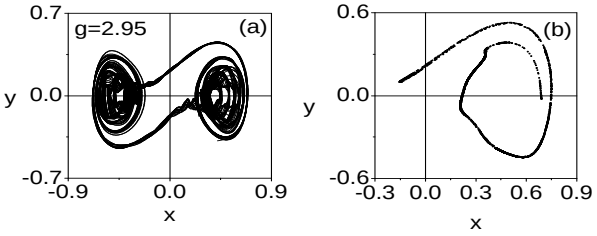

Figure 2: (a) Chaotic orbit for $g = 2.95$ and (b) the corresponding Poincaré map.

in Fig.2. A feature of the chaotic regime is the presence of windows of periodic solutions interspersed throughout the range of their existence. The period-3 window occurs for $g \in (2.495, 2.498)$, in which there is no chaotic behaviour. It is interesting, as the control parameter g is increased in the range $g \in (2.44, 2.48)$. In Fig.1(d), we also observe that the two bands of the chaotic attractor merge into a single band when the amplitude g is gradually increased beyond g=2.4632. In Fig.1(d), we can see that for fixed f=0.2, when g is increased through g=2.4750, the chaotic bands start to merge into a large one. Another type of bifurcation which is seen in Fig.1(d) is the occurrence of sudden widening or sudden increase in the size of the attractor at g=2.8012.

Fig.3(a) shows the bifurcation phenomenon for $g \in [2.490, 2.500]$. We see that just above $g_c = 2.49462$, there is a stable period-3T, while just below g_c there is chaos. We have observed that the system (Eq.(3)) also admits the intermittency route to chaos for suitable range of parameters. For example, we have observed that for f=0.2 and P=2.0, and g in the range $g \in (2.49462, 2.49458)$, the type-I intermittency occurs through a transition from the period-3 window to chaos via the intermittency (type-I) across the saddle node boundary ($g = 2.49462$). The intermittency signature is shown in Fig.3(b) and Fig.3(c) where the periodic oscillations are interrupted by intermittent amplitude bursts in the range $g \in (2.49462, 2.49458)$ as g is decreased, with further decrease in the amplitude g, the system gives birth to fully developed chaos which is shown in Fig.3(d).

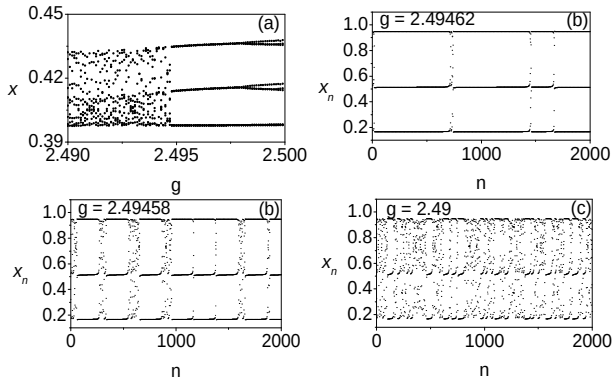

Figure 3: (a) Bifurcation diagram of the system (Eq.(3)) in the intermittency region. (b-d) $x(n)$ versus n, illustrating the intermittency route to chaos.

2.2 Hysteresis

In this section, we numerically analyze the occurrence of another dynamical behaviour such as the hysteresis phenomenon, that is, the possibility of jumping through the coexistence of attractors in a way that is not reversible when we fix a parameter back to its original value. It is present in the mechanical system, electromagnetism, chemical kinetics, astrochemical cloud models and nonlinear optics. In particular, the hysteresis phenomenon is observed in the generalized Ueda oscillator [14], modified Chua's circuit model [15], classical Morse oscillator [16] and the experimental study of Colpitt's oscillator [17]. The system (Eq.(3)) is found to show hysteresis for several ranges of values of the parameters. We give an example, with f=0.2, P=2.0 and g=1.0,P=2.0. Fig.4(a) shows the bifurcation behaviour for $g \in [1.5, 3.0]$ where g is varied from 1.5 in the forward direction. Fig.4(b) is obtained by varying g in the reverse direction from the value 3.0. Different bifurcation patterns are followed in Fig.4(a) and Fig.4(b). That is, the system (Eq.(3)) exhibits the hysteresis behaviour when the control parameter g is varied smoother from a small to a larger and then to a small value. In a similar manner, we can observe the hysteresis phenomenon, when g is fixed at 1.0, P=2.0, while f is varied from a small value. Hysteresis is realized when f is varied in the forward and reverse directions in the interval $f \in [0.8, 1.2]$, which is shown in Fig.4(c) and Fig.4(d). As shown in Fig.4, the presence of hysteresis and the coexistence of multiple attractors allow us to change the behaviour of the system (Eq.(3)) from chaos to regular by increasing the amplitudes f and g from a small to larger value to a smaller value. The suppression and enhancement of chaos are also observed which is clearly evident in Fig.4(a-d).

2.3 Vibrational resonance (VR)

In a nonlinear dynamical system driven by a biharmonic signal consisting of the low- and high-frequencies ω and Ω with $\Omega >> \omega$, when the amplitude g or frequency Ω of the high-frequency signal is varied, the response amplitude at the low-frequency ω exhibits a resonance. This high-frequency induced resonance is called the Vibrational Resonance (VR). Landa and McClintock [18] first reported the VR in a bistable system. Later on, a theoretical treatment for analyzing the VR has been proposed by Gitterman [19].

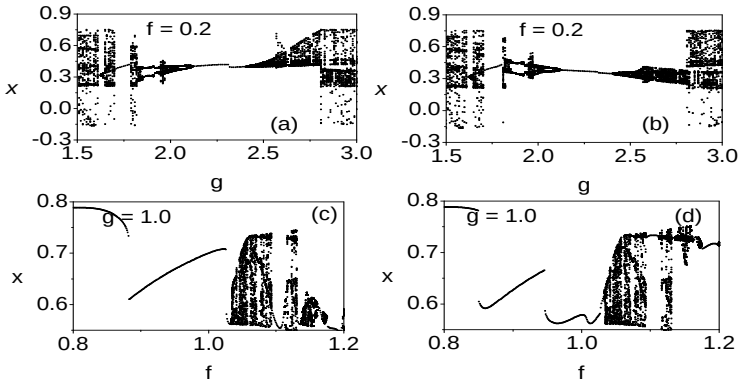

Figure 4: Bifurcation diagrams: (a) g is varied in the forward direction from zero with $f = 0.2$. (b) g is varied in the reverse direction from 3.0 with $f = 0.2$. Bifurcation diagrams: (c) f is varied in the forward direction from zero with $g = 1.0$. (d) f is varied in the reverse direction from 1.2 with $g = 1.0$. The values of the other parameters in Eq.(3) are $P = 2.0, \alpha = 1.0, \beta = 5.0, \omega = 0.1, \Omega = 5.0$ and $\gamma = 0.4$.

After these seminal works, the features of this resonance have been studied theoretically, numerically and experimentally in a variety of systems [20, 21].

In addition to the hysteresis behaviour, the system described by Eq.(3) also exhibits the phenomenon of VR, when the amplitude g and frequency Ω of the high-frequency signal are varied. To quantify the occurrence of the VR, we use response amplitude (Q) of the system (Eq.(3)) at the signal frequency ω. The system (Eq.(3)) can be numerically integrated using the fourth-order Runge-Kutta method with the time step size $T = (2\pi/\omega)/1000$. The first 10^3 drive cycles are left as transient and the values of $x(t)$ correspond to the response amplitude (Q). From the numerical solution of $x(t)$, the response amplitude is computed through with $T = 2\pi/\omega$ being the period of the response and n taken as 500.

$$Q = \sqrt{Q_s^2 + Q_c^2}/f, \tag{5a}$$

where

$$Q_s = \frac{2}{nT}\int_0^{nT} x(t)\sin(\omega t)dt, \tag{5b}$$

$$Q_c = \frac{2}{nT}\int_0^{nT} x(t)\cos(\omega t)dt. \tag{5c}$$

First, we show the occurrence of the VR due to the control parameter g for a few values of the damping exponent P with $f = 0.2$. The variation of numerically computed Q against the control parameter g for three fixed values of P, namely, $P = 0.9, 1.0$ and 1.1 is shown in Fig.5(a). The values of other parameters are fixed as $\alpha = 1.0, \beta = 5.0, \gamma = 0.4$, ω=0.1, Ω=5.0 and $f = 0.2$. In Fig.5(a), for $P = 0.9, 1.0$ and 1.1, the response amplitude Q is found to be maximum at $g = 9.5, 8.95$ and 8.0, respectively. The first striking result is that the maximum of the resonance curve increases as P increases and at the same time, its location is shifted towards a lower value of the high-frequency amplitude g. Fig.5(b) shows the variation of numerically computed Q against the control parameter

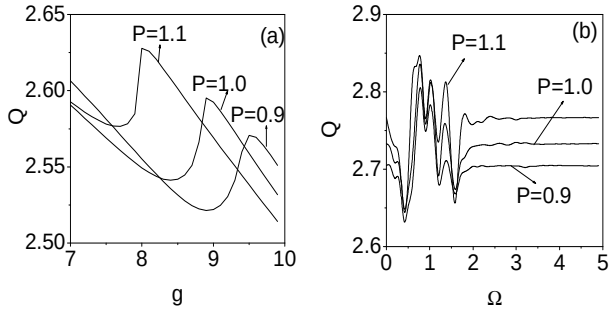

Figure 5: (a) Response amplitude Q versus g with $f = 0.2$. (b) Response amplitude Q versus Ω with $f = 0.2$ for three values of P, namely, $P = 0.9, 1.0, 1.1$. The other parameters values are $\alpha = 1.0, \beta = 5.0, \gamma = 0.4, \omega = 0.1$ and $\Omega = 5.0$.

Ω for three values of $P = 0.9, 1.0, 1.1$, respectively. For all the values of P, multiple resonances take place in the intervals $0.5 < \Omega < 2.0$ and no resonance is observed in the intervals $0 < \Omega < 0.5$ and $2.0 < \Omega < 5.0$, which is clearly evident in Fig.5(b). At $\Omega = 0.975$, the maximum value of the response amplitude Q occurs for all the values of P.

3 Dynamical Behaviours of the System with WBFM Signal

3.1 Bifurcations and chaos

For our numerical simulations, we fix the same parametric values as those previously used in the system (Eq.(3)). Fig.6 shows the bifurcation diagram for three fixed values of P, namely, P=1.0,1.5 and 2.0 with f=0.2. Fig.6(a) shows the bifurcation pattern where f is fixed at f=0.2 and P=1.0, while g is varied. As g is increased from zero, a stable period-$T(= (2\pi/\omega))$ orbit occurs which persists up to g=0.76231 and then it loses its stability giving birth to a chaotic orbit. At f=0.86275, the chaotic orbit suddenly disappears and the long-time motion settles to a periodic orbit. Fig.6(b) corresponds to P=1.5 and f=0.2 when the control parameter g is smoothly varied, the system (Eq.(4)) starts with a chaotic motion followed by the reverse period-doubling and periodic windows. The periodic behaviour is observed for $0.7625 < g < 0.86275$. When the parameter g is further increased from g=0.86275 one finds that the chaotic orbits persist for a range of g values. At g=0.96472, the chaotic motion suddenly disappears and the long-time motion settles to a periodic behaviour. The bifurcation diagram corresponding to P=2.0 and $g \in [0, 2]$ with f=0.2 is shown in Fig.6(c). When the control parameter g is smoothly varied, the system (Eq.(4)) starts with period-3T orbit followed by a chaotic orbit, periodic bubble orbit and reverse period-doubling bifurcation. At g=0.96472, the chaotic motion disappears and the long-time motion settles to a periodic behaviour. Magnification of a part of the bifurcation diagram of Fig.6(c) is shown in Fig.6(d). This figure clearly shows the reverse period-doubling bifurcation, periodic bubble orbit, and chaotic orbit. For clarity, the chaotic orbit in the $(x - \dot{x})$ plane and the strange attractor in the Poincaré map of the system driven by the WBFM signal is presented in Fig.7. It is important to note that no hysteresis behaviour has been detected while checking all the bifurcation diagrams (Fig.6) in the system (Eq.(4)). But these bifurcation diagrams show

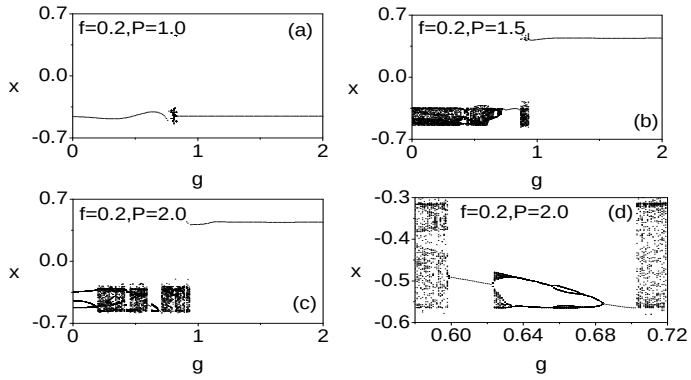

Figure 6: (a-c) Bifurcation diagrams for a few values of P with $f = 0.2$. (d) Magnification of a part of the bifurcation diagram of Fig.6(c). The other parameters values are $\alpha = 1.0,\ \beta = 5.0,\ \gamma = 0.4,\ \Omega = 5.0$ and $\omega = 0.1$.

a great number of coexisting attractors (chaotic domain) intermingled with imbricated windows made up of periodic windows of different periodicity, period doubling of both types, periodic bubbles, reverse period doubling and sudden chaos.

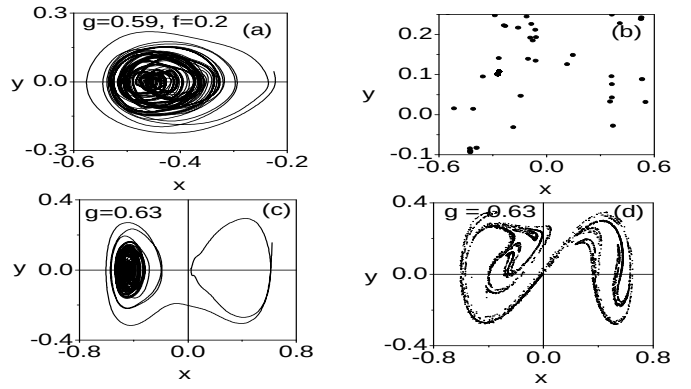

Figure 7: (a) One band chaotic orbit at $g = 0.59$ and (b) the double band chaotic orbit at $g = 0.63$. Ths corresponding Poincaré maps are shown in Figs.7(b) and 7(d).

3.2 Vibrational resonance

In order to analyze the occurrence of the VR in the system (Eq.(4)) we treat g and Ω as the control parameters. The response amplitude (Q) is calculated from the Eq.(5a).

When the system is driven by the WBFM signal, the variation of numerically computed Q with g and Ω is shown in Fig.8. Fig.8(a) shows the variation of numerically computed Q against the control parameter g for f=0.1 and P=0.1, 0.5 and 1.0. For all the values of P, as g increases from 0, the value of Q increases and reaches a maximum value at $g = g_{VR} = 6.05$ and then decreases with further increase in g. For $P = 0.1,\ 0.5$

and 1.0, the single resonance is observed at $g = 6.05$ with different $Q_{max} = 0.541,\ 0.495$ and 0.5. Fig.8(b) illustrates the variation of numerically computed Q with Ω for a few values of P. The maximum value of peak is detected at three places for $P = 0.1$ and two places at $P = 1.0$ and multiple peaks are observed for $P = 0.5$, which are clearly evident in Fig.8(b).

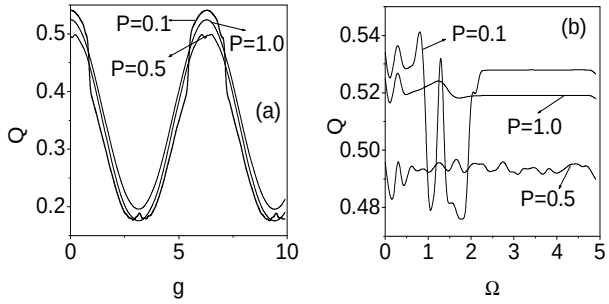

Figure 8: (a) Response amplitude Q versus g with $f = 0.1$. (b) Response amplitude Q versus Ω with $f = 0.1$ for three values of P, namely, $P = 0.1,\ 0.5,\ 1.0$. The other parameter values are $\alpha = 1.0,\ \beta = 5.0,\ \gamma = 0.4,\ \omega = 0.1$ and $\Omega = 5.0$.

4 Conclusions

This paper reports the dynamics of a nonlinearly damped Duffing-Van der Pol oscillator driven by a frequency modulated signal as a function of the amplitudes of the signal and damping exponent. We considered both signals such as NBFM and WBFM to study the dynamics of the system numerically. We demonstrated the effect of the amplitudes f and g on the dynamics of the system with other parameters at a constant value. With the variation of the amplitudes of the signal, the system exhibits period-doubling and reverse period-doubling bifurcations, periodic windows, period bubbles, hysteresis, vibrational resonance and chaotic orbits. Our results reveal many striking departures from the behaviour of a linearly damped system with the FM signal. It is also found that the FM signal suppresses the critical chaotic behaviour in some parameter ranges. The basic properties of the dynamics of the system are analyzed by the bifurcation diagram, phase portrait, Poincaré map and resonance plot. The additional features of the system in terms of coherence resonance, parametric resonance, Ghost vibrational resonance etc, deserve further study.

References

[1] J. Guckenheimer and P. Holmes. *Nonlinear Oscillations, Dynamical Systems and Bifurcation of Vector Fields*. Springer, New York, 1983.

[2] M. Lakshmanan and S. Rajasekar. *Nonlinear Dynamics, Integrability, Chaos and Patterns*. Springer, Berlin 2003.

[3] M. V. Sethu Meenakshi, S. Athisayanathan, V. Chinnathambi and S. Rajasekar. Horseshoe Dynamics in Fractionally Damped DVP Oscillator Driven by Nonsinusoidal forces. *Int. J. Nonlinear Science* **27** (2019) 81–94.

[4] S. Mukhopadhyay, B. Demircioglu and A. Chatterjee. Quantum Dynamics of a Nonlinear Kicked Oscillator. *Nonlinear Dynamics and Systems Theory* **11** (2) (2011) 173–182.

[5] A. K. Cheib,V. E. Puzyrov and N. V. Savchenko. Analysis of the Dynamics of a Two-degree-of-Freedom Nonlinear Mechanical System Under Harmonic Excitation. *Nonlinear Dynamics and Systems Theory* **20** (2) (2020) 168–178.

[6] K. Khachnaoni. Homoclinic Orbits For Damped Vibration System With Small Forcing Terms. *Nonlinear Dynamics and Systems Theory* **18** (1) (2018) 80–91.

[7] J. Kyziol and A. Okninski. The Duffing-Van der Pol Equation: Metamorphoses of Resonance Curves. *Nonlinear Dynamics and Systems Theory* **15** (1) (2015) 25–31.

[8] S. Gurubaran, B. R. D. Nayagam, V. Ravichandran, V. Chinnathambi and S. Rajasekar. Vibrational Resonance in the Classical Morse oscillator driven by Narrow-band and Wide-band frequency modulated signal. *J. Pure. App. Chem. Res.* **5** (3) (2016) 131–141.

[9] M. V. Sethu Meenakshi, S. Athisayanathan, V. Chinnathambi and S. Rajasekar. Effect of Narrow Band Frequency Modulated Signal on Horseshoe Chaos in Nonlinearly Damped Duffing-vander Pol Oscillator. *Annual Review of Chaos theory, Bifurcation and Dynamical Systems* **7** (2017) 41–55.

[10] V. Balashunmuga Jothi, B. Bhuvaneshwari, S. Kavitha and V. Chinnathambi. Vibrational Resonance in Two-coupled DVP oscillator Driven by FM signal. *Sadakath research journal* **6** (2019) 23–30.

[11] J. P. Baltanas, J. L. Trueba and M. A. F. Sanjuan. Energy Dissipation in a Nonlinearly Damped Duffing Oscillator. *Physica D* **159** (2001) 22–34.

[12] M. V. Sethu Meenakshi, S. Athisayanathan, V. Chinnathambi, and S. Rajasekar. Effect of Fractional Damping in Double-well DVP oscillator Driven by Different Sinusoidal Forces. DE GRUYTER, http://doi.org/10.1515/ijnsns-2016-0165, *Int. J. Nonlinear Science and Numerical Simulation* (2019) 1–10.

[13] M. Borowice, G. Litak and A. Syta. Vibration of Duffing Oscillator: Effect of Fractional Damping. *Shock vibration* **14** (2007) 29–36.

[14] K. Sun, A. Di-li Duo Li-Kun, Y. Dong, H. Wang and K. Zhong. Multiple Coexisting Attractors and Hysteresis in the Generalized Ueda Oscillator. *Mathematical Problems in Engineering* Article ID.256092, (2013) [DOI:10.1155/2013/256092].

[15] K. Abirami, S. Rajasekar, M. A. F. Sanjuan. Vibrational and Ghost Vibrational Resonance in a Modified Chua's Circuit Model Equation. *Int. J. Bifur. Chaos* **24** (2014) 1430031.

[16] S. Guruparan, V. Ravichandran, S. Selvaraj, V. Chinnathambi and S. Rajasekar. Coexistence of Multiple Attractors, Hysteresis and VR in the Classical Morse Oscillator Driven by an AM Signal. *Ukraine J. of Physics* **62** (1) (2017) 51–59.

[17] O. de Feo and G. Mario Maggio. Bifurcations in the Colpitts Oscillator from Theory to Practice. *Int. J. Bifur. Chaos* **13** (2003) 2917–2934.

[18] P. S. Landa and P. V. E. McClintock. Vibrational Resonance. *J. Phys. Math. Gen.* **33** (2000) L433–L438.

[19] M. Gitterman. A Bistable Oscillator Driven by Two Periodic Fields. *J. Phys. A: Math. Gen.* **34** (2001) L355–L358.

[20] S. Jeyakumari, V. Chinnathambi, S. Rajasekar and M. A. F. Sanjuan. Vibrational Resonance in an asymmetric Duffing Oscillator. *Int. J. Bifur. Chaos* **21** (2011) 275–286.

[21] K. Abirami, S. Rajasekar and M. A. F. Sanjuan. Vibrational Resonance in a Harmonically Trapped Potential System. *Commun. Nonlinear Sci. Numer. Simulat* **47** (2017) 370–378.